# 21 cm limits on decaying dark matter and primordial black holes

Steven J. Clark,[1,*] Bhaskar Dutta,[1,†] Yu Gao,[2,‡] Yin-Zhe Ma,[3,4,§] and Louis E. Strigari[1,‖]

[1]*Department of Physics and Astronomy, Mitchell Institute for Fundamental Physics and Astronomy, Texas A&M University, College Station, Texas 77843-4242, USA*

[2]*Key Laboratory of Particle Astrophysics, Institute of High Energy Physics, Chinese Academy of Sciences, Beijing 100049, China*

[3]*School of Chemistry and Physics, University of KwaZulu-Natal, Westville Campus, Private Bag X54001, Durban 4000, South Africa*

[4]*NAOC–UKZN Computational Astrophysics Centre (NUCAC), University of KwaZulu-Natal, Durban 4000, South Africa*

(Received 30 March 2018; published 8 August 2018)

Recently the Experiment to Detect the Global Epoch of Reionization Signature reported the detection of a 21 cm absorption signal stronger than astrophysical expectations. In this paper we study the impact of radiation from dark matter (DM) decay and primordial black holes (PBHs) on the 21 cm radiation temperature in the reionization epoch, and impose a constraint on the decaying dark matter and PBH energy injection in the intergalactic medium, which can heat up neutral hydrogen gas and weaken the 21 cm absorption signal. We assume a strong coupling limit in the Lyman-$\alpha$ background and consider decay channels DM $\to e^+e^-, \gamma\gamma$, $\mu^+\mu^-$, $\tau^+\tau^-$, $b\bar{b}$ and the $10^{15-17}$ g mass range for primordial black holes, and require that the heating of the neutral hydrogen does not negate the 21 cm absorption signal. For $e^+e^-$, $\gamma\gamma$ final states and PBH cases we find strong 21 cm bounds that can be more stringent than the current extragalactic diffuse photon bounds. For the DM $\to e^+e^-$ channel, the lifetime bound is $\tau_{\rm DM} > 10^{27}$ s for sub-GeV dark matter. The bound is $\tau_{\rm DM} \geq 10^{26}$ s for the sub-GeV DM $\to \gamma\gamma$ channel and reaches $10^{27}$ s for MeV DM. For $b\bar{b}$ and $\mu^+\mu^-$ cases, the 21 cm constraint is better than all the existing constraints for $m_{\rm DM} < 30$ GeV where the bound on $\tau_{\rm DM} \geq 10^{26}$ s. For both DM decay and primordial black hole cases, the 21 cm bounds significantly improve over the cosmic microwave background damping limits from Planck data.

DOI: 10.1103/PhysRevD.98.043006

## I. INTRODUCTION

Recently the Experiment to Detect the Global Epoch of Reionization Signature (EDGES) reported the observation of 21 centimeter absorption lines at high redshift $z = 15$–$20$ [1], with a best-fit neutral hydrogen spin temperature $T_{\rm S}$ much lower than conventional astrophysical expectations, leading to strong absorption signals [1]. If confirmed, the abrupt lowering of $T_{\rm S}$ relative to the cosmic microwave background (CMB) temperature $T_{\rm CMB}$ near $z \sim 20$ has been interpreted [1,2] as due to the recoupling of $T_{\rm S}$ to the hydrogen gas temperature $T_{\rm G}$ by the Wouthuysen-Field effect [3,4], where a lower-than-standard hydrogen gas temperature has been proposed that may arise from cooling effects [2] via interaction with hypothetical particles. Fulfilling such a role, potential interactions between baryons and cold dark matter (DM) have been studied and constrained [5–11].

From another perspective, the observation of a 21 cm signal also places a bound [12] on hypothetical processes that are capable of heating up the intergalactic medium (IGM) prior to the reionization time, e.g., by the energy injection from the annihilation of dark matter [13–15]. In this paper we investigate such a bound on the decay of dark matter [15–21] and the Hawking radiation [22] from primordial black holes [23,24], as both processes emit high-energy electrons and photons throughout the post-recombination history of the Universe.

Beside mapping the Universe's mass distribution at high redshift, the 21 cm absorption line(s) measurement is also a potent probe of the temperature evolution in the CMB and the intergalactic medium. Before the light from the first stars ionizes the intergalactic gas, the neutral hydrogen resonantly absorbs the 1.42 GHz radiation line as the CMB passes through. This 1.42 GHz or 21 cm wavelength spectral line corresponds to the hyperfine energy split between aligning and antialigning the spin of the electron

*cla07003@physics.tamu.edu
†dutta@physics.tamu.edu
‡gaoyu@ihep.ac.cn
§ma@ukzn.ac.za
‖strigari@physics.tamu.edu

 © 2018 American Physical Society

and that of the nucleus in the ground state of the neutral hydrogen, which form a spin-0 singlet and a spin-1 triplet. The population ratio between the triplet and singlet states is described by the spin temperature as $N_1/N_0 = 3e^{-0.068K/T_S}$. The 21 cm absorption intensity from the radiation background, i.e., the CMB, is given by the brightness temperature [25],

$$T_{21} \approx 0.023\ \mathrm{K} \cdot x_{\mathrm{H_I}}(z) \left(\frac{0.15}{\Omega_m} \cdot \frac{1+z}{10}\right)^{\frac{1}{2}} \frac{\Omega_b h}{0.02} \left(1 - \frac{T_{CMB}}{T_S}\right), \tag{1}$$

where $x_{\mathrm{H_I}}$ is the neutral ($\mathrm{H_I}$) fraction of the intergalactic hydrogen gas. For redshift $z \geq 20$ prior to reionization time, $x_{\mathrm{H_I}} \simeq 1$ in standard astrophysics. $\Omega_m$ and $\Omega_b$ are the total matter and baryon fractions of the critical energy density of the Universe, and $h$ is the Hubble constant in units of 100 $\mathrm{km\,s^{-1}\,Mpc^{-1}}$. The latest precision measurements of these cosmological parameters are given by the Planck experiment [26]. With the presence of neutral hydrogen $x_{\mathrm{H_I}} > 0$ and a colder spin temperature than the radiation background, $T_S < T_{CMB}$, the absorption feature in the CMB will emerge with $T_{21} < 0$.

The hydrogen atoms decouple from the CMB at $z \sim 200$. The background radiation temperature scales with redshift as $T_{CMB} = 2.7\ \mathrm{K} \cdot (1+z)$, while the matter temperature scales as $(1+z)^2$ and cools faster than the CMB after decoupling. Hence for the hydrogen gas its $T_S$ and $T_G$ drop below $T_{CMB}$ during the cosmic "dark age," as shown in Fig. 1. The CMB photons can still flip the $\mathrm{H_I}$ hyperfine states and slowly bring $T_S$ closer to $T_{CMB}$, and in this period we typically expect $T_G < T_S < T_{CMB}$. Entering the reionization epoch, the Lyman-$\alpha$ emissions from stars recouple $T_S$ to $T_G$ through the Wouthuysen-Field effect,

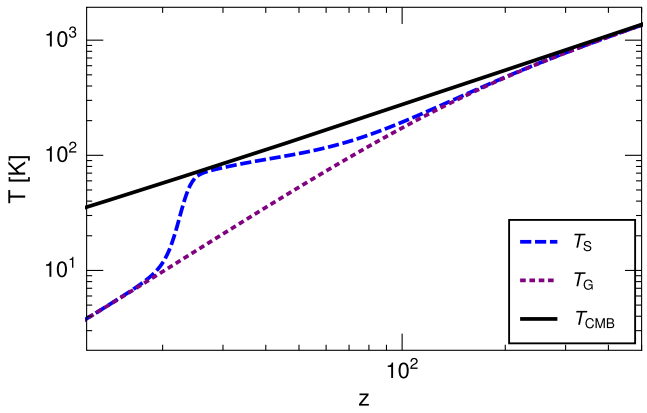


FIG. 1. $T_G, T_S$ and $T_{CMB}$ evolution in standard astrophysics without the energy injection from dark matter and black holes. $T_S$ approaches $T_{CMB}$ after the $z \sim 200$ decoupling, suppressing the 21 cm absorption until $T_S$ recouples to $T_G$ after the formation of the first stars.

and $T_S$ demonstrates a rapid drop to the colder $T_G$. This leads to a drop in $T_{21}$ and the expectation of a 21 cm absorption signal. EDGES measured a rapid lowering of $T_S$ at $z \simeq 21$, that would require $T_S \simeq T_{CMB}$ to be reached before $z \simeq 21$, and $T_S$ quickly recouples to $T_G$ by $z \sim 17$–$18$ [1]. While the 21 cm absorption signal prior to $z \sim 14$ is consistent with the cosmic reionization picture [27], the maximal signal strength $T_{21} = -500$ mK [1] at $z = 15$–$20$ is more than twice compared to the expectation from standard astrophysics. The central redshift of the $T_{21}$ trough is earlier than expected and indicates an enhanced star formation rate in galaxies [28]. The flat shape of $T_{21}(z)$ in this redshift range is also unaccounted for in a standard evolution process [1]. Reference [2] reported this low $T_{21}$ result as a $3.8\sigma$-strong absorption excess, and that the widened gap between $T_S$ from $T_{CMB}$ may arise from new physics.

However, for radio astronomy observations, the foreground contamination is at least 4 orders of magnitude higher than the 21 cm brightness temperature. This makes it extremely tricky to remove and measure the underlying signal. In Ref. [1], the EDGES group used the polynomial foreground model to fit the Galactic synchrotron and atmospheric signal in frequency space and remove it. But there could be some low-level foreground or systematics in the system that can potentially bias the results. It is also known that the low-frequency range of the CMB has potentially large radiation backgrounds [29–31]. The EDGES data can be tested and verified by future 21 cm experiments like PRIZM [32], HERA [33], LEDA [34], and SKA [35]. Here, we adopt a similar approach as in Ref. [12], that such a detection of strong 21 cm absorption by EDGES would constrain the amount of accumulated high-energy particle injection that could have heated up $T_G$ by the reionization epoch, which would narrow down the difference between $T_S$ and $T_{CMB}$ for $z = 15$–$20$ and cause a significant reduction in the 21 cm absorption signal. We will explore this constraint in light of steady electron and/or photon injection from decaying particle dark matter and evaporating black holes, and compare their lifetime bounds to other current limits. In the case of dark matter, we focus on the energy injection's heating effect and do not consider the direct scattering between dark matter and hydrogen gas, as this scattering is not necessarily significant in the minimal dark matter decay scenario.

## II. ENERGY INJECTION EFFECTS

Decaying dark matter particles with a lifetime much longer than the age of the Universe can be a steady source of Standard Model (SM) particles. The stable particles from such an injection—the photons, electrons/positrons and a generally low fraction of (anti)protons—can collide with and deposit energy to the intergalactic medium. The main effects from such energy deposition include enhanced ionization of hydrogen, leading to corrections in $x_e, x_{\mathrm{H_I}}$,

and a higher gas temperature $T_G$, especially at low redshift as the energy injection can build up over time. A higher ionization fraction $x_e$ leads to earlier reionization and more damping in the CMB's temperature and polarization correlation spectra; see Refs. [36–39] for recent studies with the Planck data. For 21 cm measurements, the corrections to both $x_e$ and $T_G$ can affect $T_{21}$, especially at a time when $T_S$ recoupled to $T_G$. A reasonable choice is at the central redshift $z \simeq 17$ where EDGES detected absorption signals. By requiring that the heating from new physics raises the radiation temperature ($\Delta T_{21}$) no more than 100 or 150 mK, this limit corresponds to a less than half or $3/4$ suppression of the standard astrophysical $T_{21} = -200$ mK absorption strength. In standard astrophysics this temperature rise can wipe out or greatly suppress the 21 cm absorption signal. It is also larger than EDGES's $T_{21}$ $1\sigma$ up-fluctuation uncertainty (+200 mK at the 99% confidence level [1]).

The $\Delta T_{21} = +100$ or $+150$ mK limits are based on the temperature evolution by the standard astrophysical processes, and should be considered as proof-of-principle estimates for new physics' heating effect on the IGM in light of a 21 cm signal discovery. As EDGES measured a stronger 21 cm signal than that from standard astrophysics, if hypothetical gas cooling also exists, it could partially negate the effect of heating processes and the same $\Delta T_{21}$ would require a larger energy injection rate. In the case of DM, gas cooling demands a prohibitive DM-baryon scattering cross section [6,7] with a limited DM mass range. Under the minimal coupling assumptions, a $10^{24-26}$ s decay lifetime is usually mediated by effective interactions that are too weak to facilitate sufficient DM-baryon scattering; thus additional DM-SM coupling structures would become necessary to make the DM's cooling effect significant, which introduces more modeling assumptions on the DM. In this paper we restrict to a minimal DM decay scenario for a generic lifetime constraint. Also, the potentially large uncertainty in the low-frequency range of the cosmic radiation field [29–31] can lead to a significant correction to the 21 cm absorption rate, which would also affect the required amount of energy-injection heating accordingly. Alternative new physics mechanisms and assessments of the radiation field background can be probed or improved using future experiments. Bearing these caveats in mind, we proceed to the IGM heating calculations from dark matter decay and black hole evaporation.

### A. Decaying dark matter

The decay of dark matter is insensitive to the small-scale matter density distribution and gives a steady energy injection rate,

$$\frac{dE}{dVdt} = \Gamma_{DM} \cdot \rho_{c,0}\Omega_{DM}(1+z)^3, \tag{2}$$

where $\Gamma$ is the dark matter decay width, and $\rho_{c,0}$ is the current critical density of the Universe. In comparison to the $(1+z)^6$ redshift dependence in the DM annihilation case, the injection rate from DM decay drops much slower than that in annihilation, and can be more significant at lower $z$.

The photons and electrons are injected at high energy that can typically reach up to $O(10^{-1})M_{DM}$. They gradually lose energy by interacting [40–42] with the intergalactic medium via ionization, Lyman-$\alpha$ excitations, gas temperature heating, as well as scattering off the background continuum photons that were studied in Ref. [43] as another explanation of the EDGES data with a heated photon radiation background. Being relativistic, these particles may take a long time to deposit all their energy into the environment. Each energy deposition channel's rate will accumulate contributions from injections at earlier times.

The energy deposition introduces additional terms in the evolution of the ionization fraction and the hydrogen temperature:

$$\frac{dx_e}{dz} = \left.\frac{dx_e}{dz}\right|_{orig} - \frac{1}{(1+z)H(z)}[I_{X_i}(z) + I_{X_\alpha}(z)], \tag{3}$$

$$\frac{dT_G}{dz} = \left.\frac{dT_G}{dz}\right|_{orig} - \frac{2}{3k_B(1+z)H(z)}\frac{K_h}{1+f_{He}+x_e}. \tag{4}$$

In the additional terms, $f_{He}$ is the helium fraction in the intergalactic medium, and $k_B$ and $H(z)$ are the usual Boltzmann constant and the Hubble parameter. The $I_{X_i}(I_{X_\alpha})$ factors correspond to the energy deposition into ionization from the hydrogen ground (excited) states. $K_h$ takes account of the heating of intergalactic gas. These factors are related to the energy injection rate by

$$I_{X_i}(z) = \frac{f_i(E,z)}{n_H(z)E_i}\frac{dE}{dVdt}, \tag{5}$$

$$I_{X_\alpha}(z) = (1-C)\frac{f_\alpha(E,z)}{n_H(z)E_\alpha}\frac{dE}{dVdt}, \tag{6}$$

$$K_h(z) = \frac{f_h(E,z)}{n_H(z)}\frac{dE}{dVdt} \tag{7}$$

$$C = \frac{1 + K\Lambda_{2s,1s}n_H(1+x_e)}{1 + K\Lambda_{2s,1s}n_H(1-x_e) + K\beta_B n_H(1-x_e)}. \tag{8}$$

$n_H$ is the hydrogen number density, and $E_i, E_\alpha$ are the electron energy levels at the ground and excited states of the hydrogen atom. $\Lambda_{2s,1s}$ is the decay rate from the $2s$ to $1s$ energy level. $\beta_B$ is the effective photoionization rate, and $K = \lambda_\alpha^3/(8\pi H(z))$, with $\lambda_\alpha$ being the Lyman-$\alpha$ wavelength. $C$ is approximately the probability that an excited hydrogen

atom will decay through two-photon emission before becoming ionized. Collisional deexcitation effects are subdominant [44–46]. The redshift dependence effective efficiencies $f_{\rm i}, f_\alpha, f_{\rm h}$ represent the ratio of energy deposition into each channel to the total energy injection rate at the current redshift. These effective efficiencies $f(E,z)$ will include both species/spectrum averaging and the accumulative contribution from earlier injections, after propagating to the current redshift. Thus $f(E,z)$ has a dependence on the injection history, the cosmic-ray species and their energy at injection.

We calculate the effective efficiencies for different models based on the numerical values given in Refs. [38,42] for electron and photon effective efficiency maps. These are the only maps required as only electrons and photons can efficiently deposit energy into the intergalactic medium. Protons may also be produced if kinematically allowed, but their heating contribution can be ignored due to their subleading final-state multiplicity. Efficiency maps for other products are created by first calculating model-dependent immediate decay products. These products then undergo a decay chain that produces the spectra of stable products. This decay is assumed to occur instantaneously. Finally, the spectra are combined with the original electron and photon efficiency tables through a weighted average to create the effective efficiency map for the model [47]

$$f_c(m_{\rm DM},z)=\frac{\sum_s\int f_c(E,z,s)E(\mathrm{d}N/\mathrm{d}E)_s\mathrm{d}E}{\sum_s\int E(\mathrm{d}N/\mathrm{d}E)_s\mathrm{d}E}, \quad (9)$$

where $c$ is the channel, $s$ is the species, $f_c(E,z,s)$ is the effective efficiency for the channel and species, and $(dN/dE)_s$ is the spectrum for the species.

Equations (5)–(7) account for the energy deposit corrections to hydrogen ionization, Lyman-$\alpha$ excitation and gas heating. We do not include the effects on helium ionization and the energy loss to the photon continuum as their impact is subdominant [39].

The terms with lower script "orig" in Eqs. (3) and (4) refer to the unaltered standard evolution equations [46,48],

$$\left.\frac{\mathrm{d}x_{\rm e}}{\mathrm{d}z}\right|_{\rm orig}=\frac{C}{(1+z)H(z)}\times(x_{\rm e}^2 n_{\rm H}\alpha_{\rm B}-\beta_{\rm B}(1-x_{\rm e})e^{-h\nu_{2s}/k_{\rm B}T_{\rm G}}), \quad (10)$$

$$\left.\frac{\mathrm{d}T_{\rm G}}{\mathrm{d}z}\right|_{\rm orig}=\frac{8\sigma_{\rm T}a_{\rm R}T_{\rm CMB}^4}{3m_{\rm e}cH(z)(1+z)}\frac{x_{\rm e}}{1+f_{\rm He}+x_{\rm e}}(T_{\rm G}-T_{\rm CMB}), \quad (11)$$

where $\alpha_{\rm B}$ is the effective recombination.

We use the numerical package HyRec [48] to compute the temperature evolutions, with the energy injection corrections implemented into the evolution equations. The Wouthuysen-Field effect is added to the calculation by defining [25]

$$T_{\rm S}=\frac{T_{\rm CMB}+y_{\rm c}T_{\rm G}+y_{{\rm Ly}\alpha}T_{{\rm Ly}\alpha}}{1+y_{\rm c}+y_{{\rm Ly}\alpha}}, \quad (12)$$

$$y_{\rm c}=\frac{C_{10}}{A_{10}}\frac{T_\star}{T_{\rm G}}, \quad (13)$$

$$y_{{\rm Ly}\alpha}=\frac{P_{10}}{A_{10}}\frac{T_\star}{T_{{\rm Ly}\alpha}}, \quad (14)$$

where $A_{10}=2.85\times10^{-15}\ \mathrm{s}^{-1}$ is the transition's spontaneous emission coefficient, $C_{10}$ is the collisional deexcitation rate of the triplet hyperfine level, $P_{10}\approx1.3\times10^{-12}S_\alpha J_{-21}\ \mathrm{s}^{-1}$ is the indirect deexcitation rate due to Lyman-$\alpha$ absorption, $T_\star=h\nu_0/k_{\rm B}=0.068$ K is the Lyman-$\alpha$ energy, $T_{{\rm Ly}\alpha}$ is the Lyman-$\alpha$ background temperature (where $T_{{\rm Ly}\alpha}=T_{\rm G}$ for the period of interest), $S_\alpha$ is a factor of order unity that incorporates spectral distortions [49], and $J_{-21}$ is the Lyman-$\alpha$ background intensity written in units of $10^{-21}\ \mathrm{erg\,cm^{-2}\,s^{-1}\,Hz^{-1}\,sr^{-1}}$ and is estimated by an average of the early and late reionization results of Ref. [50].

This work does not aim at a rigorous analysis of astrophysical reionization models. Instead, we assume $T_{\rm S}$ reaches the strong coupling limit, with $J_{-21}\gg1$ [25] during EDGES' signal creation at the early redshift range $17<z<20$ of the reionization era. We model $J_{-21}$ by taking the average of the two scenarios in Ref. [50], and this assumption will qualify as a conservative constraint on the heating from new-physics energy injection: our choice $J_{-21}$ suffices for the strong coupling limit. As long as the strong coupling limit is satisfied, the $T_{\rm S}$ result and its associated new-physics constraint remain unchanged for different values of $J_{-21}$. In the case of a much lower $J_{-21}$ away from the strong coupling limit, the coupling between $T_{\rm S}$ and $T_{\rm G}$ is weaker; thus, less new-physics heating is required and the bound is strengthened.

It is also noted that we do not include the x-ray heating effects for the depth of the $T_{21}$ signal at $z\sim17$, which would become dominant at later redshifts and closes the $T_{21}$ trough near full ionization, which the EDGES measurement indicates happens at $z=14$. In this analysis we focus on the maximal $T_{21}$ strength that depends on the gas temperature at the beginning of the reionization era, and our bounds without x-ray effects are conservative as additional astrophysical heating reduces the 21 cm signal. To fully describe the $T_{21}$ features from the EDGES data, a detailed model that incorporates astrophysical heating would be needed.

We use the cosmological parameters $\Omega_{\rm m}=0.3$, $\Omega_{\rm b}=0.04$, $\Omega_\Lambda=0.7$, and $h=0.7$ throughout this work. Figure 2 illustrates the heating effect on $T_{\rm G}$ and $T_{21}$ from dark matter decay, assuming a contribution from 100% of the relic density and the DM $\to e^+e^-$ channel. The heating

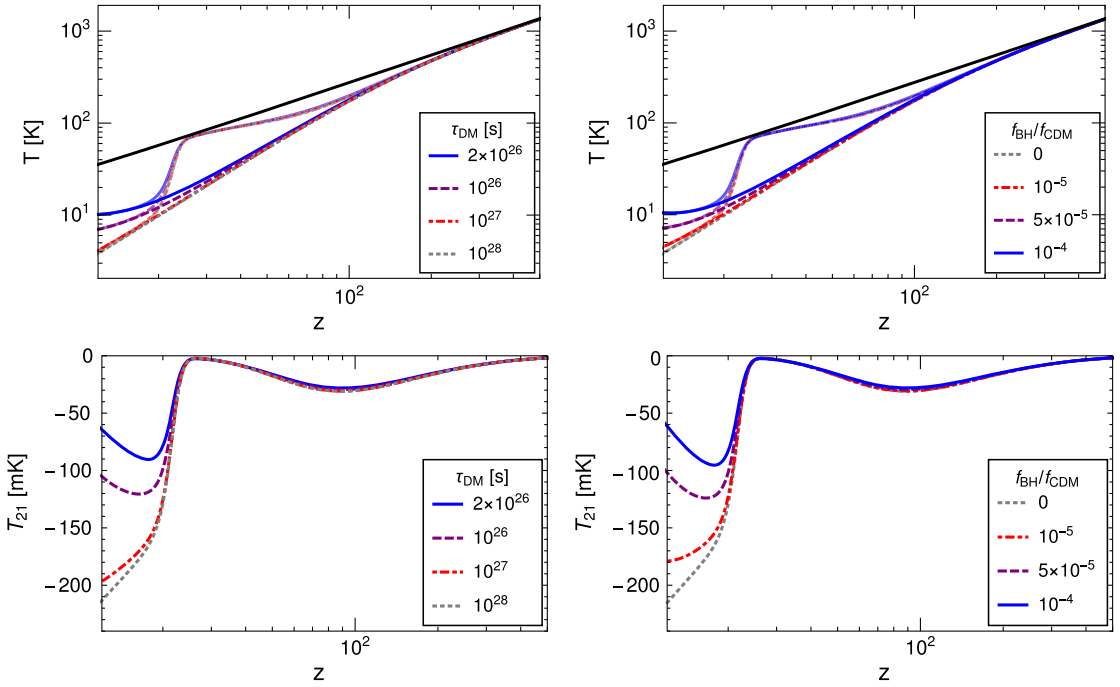


FIG. 2. Dark matter decay (left) and primordial black hole evaporation (right) effects lead to higher $T_G$ (top) and $T_{21}$ (bottom) in the reionization epoch. Here the dark matter mass is 100 GeV and decays into an $e^+e^-$ final state. The black hole mass is assumed to $10^{16}$ g. For convenience, $T_{CMB}$ (black) and $T_S$ (faded) are also shown in the $T_G$ graphs.

of neutral hydrogen becomes manifest near the reionization time. Note that variations in cosmological parameters do slightly affect the result. Cosmological parameter variation within Planck's constraint is expected to lead to an $\mathcal{O}(1)$ correction. As an example, for the best fit of Planck's TT, TE, EE + lowP data, $\Omega_m = 0.316$, $\Omega_b = 0.049$, $\Omega_\Lambda = 0.684$, and $h = 0.67$ [26], the constraints shown in Sec. III are weakened by a factor of 1.6.

### B. Primordial black holes

Another potential source of steady $e^\pm$, $\gamma$ injection is the Hawking radiation of long-lived, relatively low-mass ($M_{BH} > 10^{15}$ g) primordial black holes (PBHs). Overdensity in the early Universe can collapse into primordial black holes [51–54]. If PBH formation occurs during radiation-dominated phases, usually a horizon-sized fluctuation is needed to overcome the radiation pressure and makes overdensity growth possible, leading to a characteristic PBH size. In matter-dominated phases, however, PBH formation can be a lot more complicated. The lack of radiation pressure allows for black hole formation over a wide range of mass, and the mass profile can depend on the geometric symmetry of density fluctuations [55,56]. For a review of PBH formation and relevant constraints, see Refs. [57–59], and Ref. [60] for constraints on horizonless exotic compact objects. Also see Refs. [61–63] for recent studies of PBH formation under nonthermal conditions.

Relevant PBHs for post-recombination energy injection need to be long-lived such that their evaporation time scale is longer than the age of the Universe. PBHs with $M_{BH} > 10^{15}$ g can survive to today, and PBHs in the mass range $10^{15}$–$10^{17}$ g are subject to indirect searches for extragalactic cosmic rays [24] and CMB damping constraints [39,64,65].

A black hole of mass $M_{BH}$ loses its mass at the Hawking radiation rate [22],

$$\dot{M}_{BH} = -5.34\times10^{25}\left(\sum_i \phi_i\right) M_{BH}^{-2}\ \mathrm{g^3\ s^{-1}}, \quad (15)$$

where the coefficients $\phi_i$ are the fraction of evaporation power and sums over all particle degrees of freedom that are less massive than the BH's temperature $T_{BH} = (8\pi G M_{BH})^{-1}$. Here we use the greek letter $\phi$ to avoid confusion with the effective absorption coefficient $f_i$. The relevant emissions are photons and electrons as they can interact with the intergalactic medium. Other emission species, like neutrinos, do not deposit their energy into the intergalactic medium in an efficient manner. For each particle degree of freedom in photons and electrons, $\phi_1^\gamma = 0.06$ and $\phi_{1/2}^{e^\pm} = 0.142$ [66]. Note that these $\phi$ values are normalized to the emission of a $10^{17}$ g black hole. The PBH injection also scales as $(1+z)^3$ and depends on the abundance of black holes,

$$\frac{dE}{dVdt} = \sum_{i=\gamma,e^\pm} \phi_i \cdot \frac{\dot{M}_{BH}}{M_{BH}} \rho_{c,0}\Omega_{BH}(1+z)^3, \quad (16)$$

where $\dot{M}_{\rm BH}/M_{\rm BH} \propto M_{\rm BH}^{-3}$ is the mass loss rate. For $M_{\rm BH} \gg 10^{15}$ g, $M_{\rm BH}$ can be considered within the age of the Universe. Comparing with Eq. (2), the PBH injection rate has the same redshift dependence as that in the dark matter decay scenario. The treatment of the interaction of photons and electrons with the intergalactic medium follows the same procedure as discussed in the previous subsection. The impact on $T_{\rm G}$ and $T_{21}$ is shown in the right panels of Fig. 2 for a $10^{16}$ g mass PBH with a few sample abundances between $10^{-5}$ and $10^{-4}$ of the Universe's matter density.

## III. CONSTRAINTS FROM THE 21 CM SIGNAL

By requiring the $T_{21}$ correction to its standard astrophysical value at $z \simeq 17$ to be less than 100 and 150 mK, namely $T_{21}(z = 17) < -100$ and $-50$ mK respectively, we obtain strong constraints on the lifetime of decaying dark matter, and the maximally allowed abundance of primordial black holes.

Figure 3 illustrates the constraint on the decay lifetime $\tau_{\rm DM}$ for a DM mass of ~MeV up to 100 TeV. The constraint assumes generic two-body decay channels. The DM $\to e^+e^-$ channel is the most stringently constrained due to the

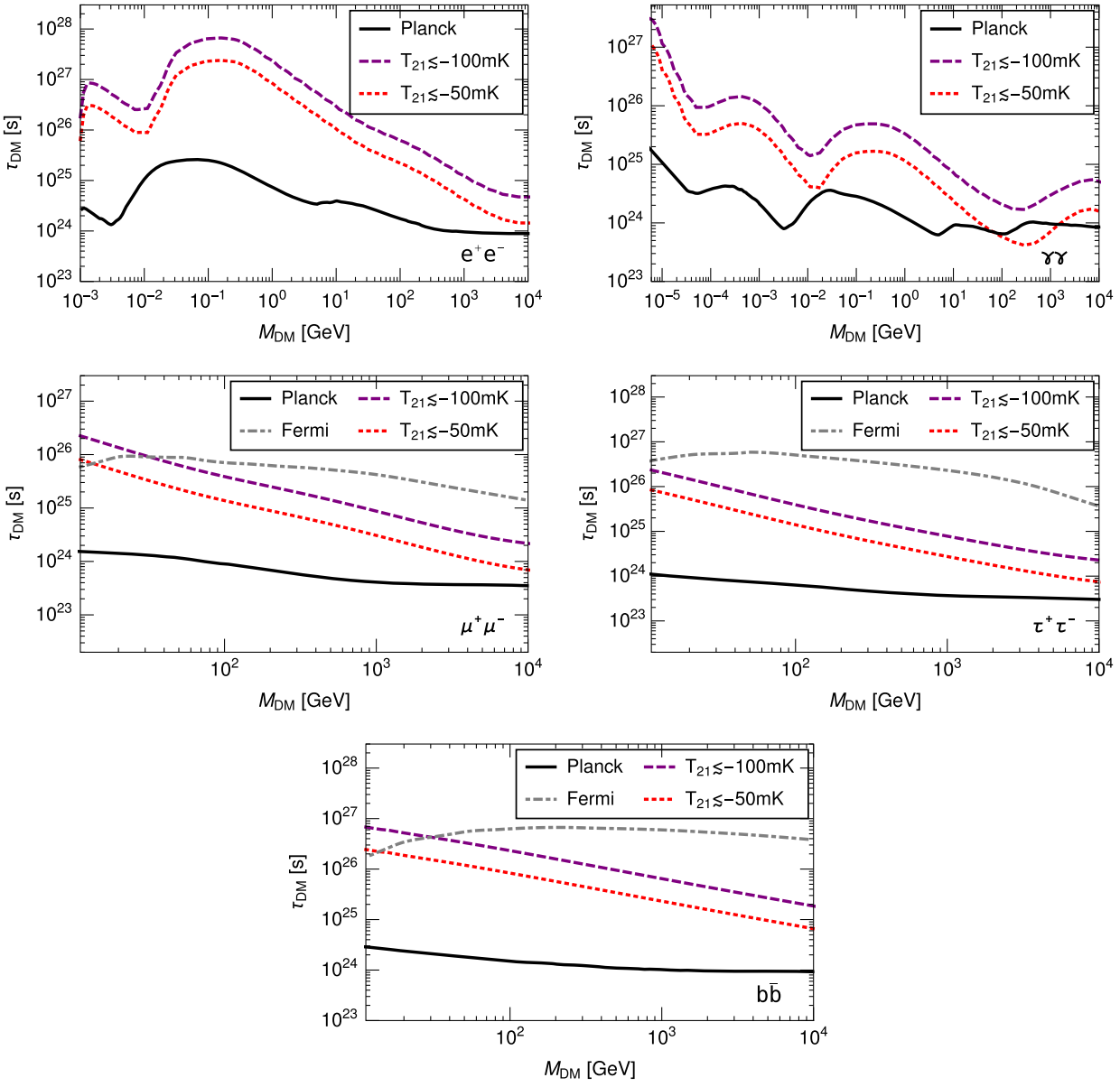


FIG. 3. 21 cm lower bounds on the dark matter decay lifetime, and primordial black hole abundance. The DM decay panels assume DM $\to e^+e^-$ (top left), DM $\to \gamma\gamma$ (top right), DM $\to \mu^+\mu^-$ (center left), DM $\to \tau^+\tau^-$ (center right), and DM $\to b\bar{b}$ (bottom) final states. Current CMB damping constraints [36] from Planck (solid) and dwarf galaxy bounds [67] from Fermi-LAT (gray dashed) are also shown for comparison.

fact that it has the highest fraction of electrons in the final state. $\mu^+\mu^-$ and $b\bar{b}$ final states are also plotted, which have lower $f(E,z)$ in comparison. $\mu^+\mu^-$, $b\bar{b}$ are also much smoother than $e^+e^-$ due to the wide spectra of stable final particles which results in most features of $f$ averaging out. As a lower energy injection requires less time to deposit its energy into the intergalactic medium, $f$ increases with lower $M_{\rm DM}$, as demonstrated in the shape of the $\tau_{\rm DM}$ constraint. This leads to a significant $\mathcal{O}(10^{27})$ s bound for the sub-GeV dark matter lifetime that is complementary to gamma-ray search limits [67,68] from Fermi-LAT data. The 21 cm bound is also stronger than the CMB damping constraint from Planck [39] by more than 1 order of magnitude. This indicates that the $T_{\rm S} \simeq T_{\rm G}$ in the reionization epoch is also a very sensitive test of energy injection. $\mu^+\mu^-$ and $b\bar{b}$ final states for masses above 30 GeV produce weaker bounds than Fermi-LAT's dwarf galaxy [67] and Galactic [69,70] gamma-ray measurements. $\tau^+\tau^-$ final states result in weaker bounds for all tested masses but reach comparable results at $m_{\rm DM} = 10$ GeV. However, because $e^+e^-$ produces fewer gamma rays and has a higher $f(E,z)$, it is expected to be much more constraining than Fermi-LAT. The shape of the constraints is a direct result of the effective efficiency maps discussed in Sec. II. Masses that occur near a peak absorption efficiency have a correspondingly high constraint. The shifting of the peaks between Planck and 21 cm results is due to the $z$ dependence of the effective efficiency. Dominant features present in the efficiency map shift to higher DM and lower PBH masses at late redshift and are observed in calculated maps [39,42].

Also note the enhanced lifetime in the $\gamma\gamma$ channel at injections below 0.1 MeV due to higher photon energy absorption efficiency. For $\sim$ keV DM the lifetime bound is higher than $10^{27}$ s. This bound is below the $10^{29}$ s $\cdot$ $(M_{\rm DM}/{\rm keV})$ [71] requirement for explaining the 3.5 keV x-ray excess [72]. Testing this signal would need $\mathcal{O}({\rm mK})T_{21}$ sensitivity at future measurements.

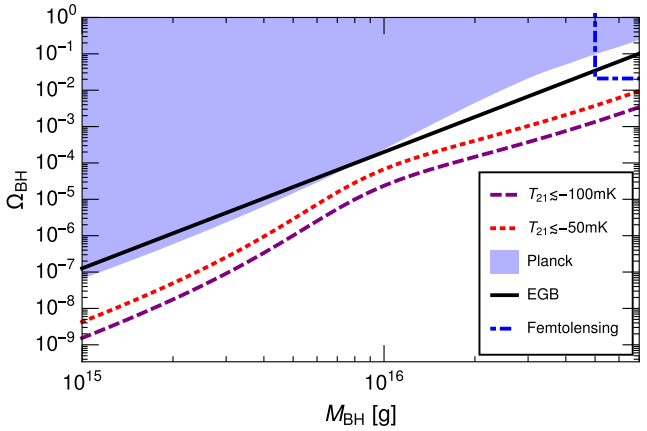


FIG. 4. 21 cm upper bounds on the primordial black hole abundance. Current CMB damping [39] (shaded), extragalactic gamma-ray background [24,39] (solid) constraints and the femtolensing excluded area [73] (top right) are also shown for comparison.

For PBHs, the injection rate $\dot{M}_{\rm BH}/M_{\rm BH} \propto M_{\rm BH}{}^{-3}$ quickly drops for higher BH masses. Also, for BH masses much higher than $10^{16}$ g, the BH temperature drops below the electron mass, reducing the amount of electron injection and the impact on the intergalactic medium's temperature. Figure 4 shows the 21-cm-constrained maximal fraction of the Universe's dark matter in the form of primordial black holes. Comparing with the CMB damping limit from Planck, the 21 cm bound is stronger by 1 order of magnitude throughout the relevant mass range.

## IV. CONCLUSION

We studied the impact of dark matter decay and PBH radiation on the 21 cm radiation temperature in the reionization epoch, in light of the recent measurement of a 21 cm absorption signal by the EDGES experiment. In this work we did not aim at resolving the deviation of EDGES's measured $T_{21}$ from the standard astrophysical expectation. Instead we imposed a conservative constraint on the historic energy injection in the intergalactic medium, by requiring that this injection does not fully wipe out or cause major correction to the 21 cm absorption signal by $z = 17$, at the middle of the redshift range where the absorption signal is expected to be the strongest.

We adopted the effective absorption efficiencies from Ref. [38] for a continuous energy deposit process from injected particles and a strong coupling limit for the astrophysical Lyman-$\alpha$ intensity during the early reionization era, and simulated the spin and gas temperatures down to redshift $z = 17$. Focusing on the maximal $T_{21}$ strength and the $z = 17$ temperature increase from DM and PBH injection, the constraint is conservative due to our choice of the Lyman-$\alpha$ model, and the fact that we neglected x-ray heating during early reionization. Our choice of $\Delta T_{21} = +150$, 200 mK benchmarks can be potentially affected if a large low-frequency radiation background is present. The bound can be scaled proportionally for different $\Delta T_{21}$ requirements.

We considered DM decay channels DM $\to e^+e^-, \gamma\gamma$, $\mu^+\mu^-, b\bar{b}$ and obtained $\tau_{\rm DM} \geq 10^{26\text{–}27}$ s bounds on the DM lifetime by requiring that the heating process increases the gas temperature to no higher than $-100$ or $-50$ mK. For $e^+e^-, \gamma\gamma$ final states and PBH cases, the 21 cm observation provides the best bound in the DM mass-lifetime parameter space. For $b\bar{b}$ and $\mu^+\mu^-$ final states, the 21 cm observation bound becomes better than all the existing constraints for $m_{\rm DM} < 30$ GeV. For $\tau^+\tau^-$ final states, constraints are similar for $m_{\rm DM} \approx 10$ GeV. In both the DM and PBH cases, the 21 cm bound is found to be better than the current CMB damping constraint from Planck data.

Since the removal of extremely large foreground from the data is difficult, the EDGES result needs to be verified

by future 21 cm experiments like PRIZM, HERA, LEDA, and SKA. If the absorption signal is verified in the future, the 21 cm absorption can prove to be a powerful probe of nonstandard heating processes. It is worth emphasizing the 21 cm signal's sensitivity to $e^{\pm}$, $\gamma$ injection in the sub-GeV energy range as demonstrated in Fig. 3. In contrast to the poor absorption efficiency at TeV or higher energy scales, the sub-GeV bound on decaying dark matter can nicely fill in the MeV–GeV range where the indirect search bounds are currently less stringent in comparison to x-ray and hard gamma-ray limits.

## ACKNOWLEDGMENTS

S. J. C. acknowledges support from NASA Astrophysics Theory grant NNX12AC71G. B. D. and L. E. S. acknowledge support from DOE Grant No. de-sc0010813. Y. G. is supported under Grant No. Y7515560U1 by the Institute of High Energy Physics, Chinese Academy of Sciences. Y. Z. M. is supported by the National Research Foundation of South Africa with Grants No. 105925 and No. 104800. We thank X-J. Bi, N. Mirabolfathi, and N. Suntzeff for discussions.

[1] J. D. Bowman, A. E. E. Rogers, R. A. Monsalve, T. J. Mozdzen, and N. Mahesh, Nature (London) **555**, 67 (2018).
[2] R. Barkana, Nature (London) **555**, 71 (2018).
[3] S. A. Wouthuysen, Astron. J. **57**, 31 (1952).
[4] G. B. Field, Proc. Ire. **46**, 240 (1958).
[5] A. Fialkov, R. Barkana, and A. Cohen, Phys. Rev. Lett. **121**, 011101 (2018).
[6] A. Berlin, D. Hooper, G. Krnjaic, and S. D. McDermott, Phys. Rev. Lett. **121**, 011102 (2018).
[7] R. Barkana, N. J. Outmezguine, D. Redigolo, and T. Volansky, arXiv:1803.03091.
[8] J. B. Muoz and A. Loeb, Nature (London) **557**, 684 (2018).
[9] S. Fraser *et al.*, arXiv:1803.03245.
[10] Z. Kang, arXiv:1803.04928.
[11] C. Jin, W. Liu, H.-B. Hu, and Y.-Q. Guo, Phys. Rev. D **97**, 123005 (2018).
[12] G. D'Amico, P. Panci, and A. Strumia, Phys. Rev. Lett. **121**, 011103 (2018).
[13] L. Zhang, X.-L. Chen, Y.-A. Lei, and Z.-G. Si, Phys. Rev. D **74**, 103519 (2006).
[14] E. Ripamonti, M. Mapelli, and A. Ferrara, Mon. Not. R. Astron. Soc. **375**, 1399 (2007).
[15] S. R. Furlanetto, S. P. Oh, and E. Pierpaoli, Phys. Rev. D **74**, 103502 (2006).
[16] X.-L. Chen and M. Kamionkowski, Phys. Rev. D **70**, 043502 (2004).
[17] S. Kasuya and M. Kawasaki, Phys. Rev. D **70**, 103519 (2004).
[18] E. Pierpaoli, Phys. Rev. Lett. **92**, 031301 (2004).
[19] Y. A. Shchekinov and E. O. Vasiliev, Mon. Not. R. Astron. Soc. **379**, 1003 (2007).
[20] M. Mapelli, A. Ferrara, and E. Pierpaoli, Mon. Not. R. Astron. Soc. **369**, 1719 (2006).
[21] E. Ripamonti, M. Mapelli, and A. Ferrara, Mon. Not. R. Astron. Soc. **374**, 1067 (2007).
[22] S. W. Hawking, Nature (London) **248**, 30 (1974).
[23] K. J. Mack and D. H. Wesley, arXiv:0805.1531.
[24] B. J. Carr, K. Kohri, Y. Sendouda, and J. Yokoyama, Phys. Rev. D **81**, 104019 (2010).
[25] M. Zaldarriaga, S. R. Furlanetto, and L. Hernquist, Astrophys. J. **608**, 622 (2004).
[26] P. A. R. Ade *et al.* (Planck Collaboration), Astron. Astrophys. **594**, A13 (2016).
[27] A. Cohen, A. Fialkov, R. Barkana, and M. Lotem, Mon. Not. R. Astron. Soc. **472**, 1915 (2017).
[28] J. Mirocha and S. R. Furlanetto, arXiv:1803.03272.
[29] D. J. Fixsen *et al.*, Astrophys. J. **734**, 5 (2011).
[30] C. Feng and G. Holder, Astrophys. J. **858**, L17 (2018).
[31] M. Pospelov, J. Pradler, J. T. Ruderman, and A. Urbano, Phys. Rev. Lett. **121**, 031103 (2018).
[32] J. B. Peterson, T. C. Voytek, A. Natarajan, J. M. J. Garcia, and O. Lopez-Cruz, in *Proceedings of the 49th Rencontres de Moriond on Cosmology, La Thuile, Italy, March 15–22, 2014*, edited by E. Auge, J. Dumarchez, and J. T. T. Vân (Moriond, Paris, 2014), p. 129.
[33] D. R. DeBoer *et al.*, Publ. Astron. Soc. Pac. **129**, 045001 (2017).
[34] D. C. Price *et al.*, arXiv:1709.09313.
[35] J. Pritchard *et al.* (EoR/CD-SWG and Cosmology-SWG), Proc. Sci., AASKA14 (**2015**) 012, [arXiv:1501.04291].
[36] T. R. Slatyer and C.-L. Wu, Phys. Rev. D **95**, 023010 (2017).
[37] T. R. Slatyer, Phys. Rev. D **93**, 023527 (2016).
[38] T. R. Slatyer, Phys. Rev. D **93**, 023521 (2016).
[39] S. J. Clark, B. Dutta, Y. Gao, L. E. Strigari, and S. Watson, Phys. Rev. D **95**, 083006 (2017).
[40] T. R. Slatyer, Phys. Rev. D **87**, 123513 (2013).
[41] K. M. Belotsky and A. A. Kirillov, J. Cosmol. Astropart. Phys. 01 (2015) 041.
[42] H. Liu, T. R. Slatyer, and J. Zavala, Phys. Rev. D **94**, 063507 (2016).
[43] Y. Yang, X. Huang, and L. Feng, arXiv:1803.05803.
[44] P. J. E. Peebles, Astrophys. J. **153**, 1 (1968).
[45] S. Galli, T. R. Slatyer, M. Valdes, and F. Iocco, Phys. Rev. D **88**, 063502 (2013).
[46] M. S. Madhavacheril, N. Sehgal, and T. R. Slatyer, Phys. Rev. D **89**, 103508 (2014).
[47] S. J. Clark, B. Dutta, and L. E. Strigari, Phys. Rev. D **97**, 023003 (2018).
[48] Y. Ali-Haimoud and C. M. Hirata, Phys. Rev. D **83**, 043513 (2011).
[49] C. M. Hirata, Mon. Not. R. Astron. Soc. **367**, 259 (2006).
[50] B. Ciardi and P. Madau, Astrophys. J. **596**, 1 (2003).

[51] S. Hawking, Mon. Not. R. Astron. Soc. **152**, 75 (1971).
[52] Y. Zel'dovich and I. D. Novikov, Astron. Zh. **43**, 758 (1966).
[53] Y. Zel'dovich and I. D. Novikov, Sov. Astron. **10**, 602 (1967).
[54] B. J. Carr and S. W. Hawking, Mon. Not. R. Astron. Soc. **168**, 399 (1974).
[55] M. Yu. Khlopov, Res. Astron. Astrophys. **10**, 495 (2010).
[56] A. G. Polnarev and M. Y. Khlopov, Soviet J. Astrophys. **25**, 406 (1981).
[57] B. Carr, F. Kuhnel, and M. Sandstad, Phys. Rev. D **94**, 083504 (2016).
[58] A. M. Green, Phys. Rev. D **94**, 063530 (2016).
[59] B. Carr, M. Raidal, T. Tenkanen, V. Vaskonen, and H. Veermae, Phys. Rev. D **96**, 023514 (2017).
[60] M. Raidal, S. Solodukhin, V. Vaskonen, and H. Veerme, Phys. Rev. D **97**, 123520 (2018).
[61] J. Georg, G. Sengor, and S. Watson, Phys. Rev. D **93**, 123523 (2016).
[62] L. Chen, Q.-G. Huang, and K. Wang, J. Cosmol. Astropart. Phys. 12 (2016) 044.
[63] J. Georg and S. Watson, J. High Energy Phys. 09 (2017) 138.
[64] V. Poulin, J. Lesgourgues, and P. D. Serpico, J. Cosmol. Astropart. Phys. 03 (2017) 043.
[65] P. Stcker, M. Krmer, J. Lesgourgues, and V. Poulin, J. Cosmol. Astropart. Phys. 03 (2018) 018.
[66] J. H. MacGibbon, Phys. Rev. D **44**, 376 (1991).
[67] M. G. Baring, T. Ghosh, F. S. Queiroz, and K. Sinha, Phys. Rev. D **93**, 103009 (2016).
[68] W. Liu, X.-J. Bi, S.-J. Lin, and P.-F. Yin, Chin. Phys. C **41**, 045104 (2017).
[69] M. Ackermann *et al.* (Fermi-LAT Collaboration), Phys. Rev. D **91**, 122002 (2015).
[70] T. Cohen, K. Murase, N. L. Rodd, B. R. Safdi, and Y. Soreq, Phys. Rev. Lett. **119**, 021102 (2017).
[71] E. Bulbul, M. Markevitch, A. Foster, R. K. Smith, M. Loewenstein, and S. W. Randall, Astrophys. J. **789**, 13 (2014).
[72] A. Boyarsky, O. Ruchayskiy, D. Iakubovskyi, and J. Franse, Phys. Rev. Lett. **113**, 251301 (2014).
[73] A. Barnacka, J. F. Glicenstein, and R. Moderski, Phys. Rev. D **86**, 043001 (2012).